The hemodynamic power of the heart differentiates normal from diseased right ventricles

Gianni Pedrizzetti [a,*], Giorgio Faganello [b], Elisa Croatto [b], Andrea Di Lenarda [b]

[a] Department of Engineering and Architecture, University of Trieste, Italy
[b] Cardiovascular Department, Azienda Sanitaria Universitaria Giuliano Isontina, Trieste, Italy

ARTICLE INFO

Article history:
Accepted 3 February 2021

Keywords:
Cardiac mechanics
Cardiac fluid dynamics
Mechanical work
Hemodynamic
Right ventricle

ABSTRACT

Cardiac mechanics is primarily described by the pressure-volume relationship. The ventricular pressure-volume loop displays the instantaneous relationship between intraventricular pressure and volume throughout the cardiac cycle; however, it does not consider the shape of the ventricles, their spatiotemporal deformation patterns, and how these balance with the flowing blood.

Our study demonstrates that the pressure-volume relationship represents a first level of approximation for the mechanical power of the ventricles, while, at a further level of approximation, the importance of hemodynamic power emerges through the balance between deformation patterns and fluid dynamics. The analysis is preliminarily tested in a healthy subject's right ventricle and two patients. Moreover, patients' geometry was then rescaled to present a normal volumetric profile to verify whether results were affected by volume size or by the spatiotemporal pattern of how that volume profile was achieved.

Results show that alterations of hemodynamic power were found in the abnormal ventricles and that they were not directly caused by the ventricular size but by changes in the ability of intraventricular pressure gradient to generate blood flow. Therefore, hemodynamic power represents a physics-based measure that takes into account the dynamics of the space-time shape changes in combination with blood flow.

Hemodynamic power is assessed non-invasively using cardiac imaging techniques and can be an early indicator of cardiac dysfunction before changes occur in volumetric measurements. These preliminary results provide a physical ground to evaluate its diagnostic or prognostic significance in future clinical studies.

1. Introduction

Last century of industrial developments featured, among others, a spread application of mechanical piston-like pumps or impellers, turbines to transfer fluids or to create energy; indeed, a large scientific effort was devoted to develop methods for their design and optimization. Recent years witnessed the development of new generations of pumping systems made with soft tissues. These probably took the lead from mammalian heart to improve understanding the various aspects of pumping function of cardiac chambers (Baillargeon et al., 2014; Pedrizzetti et al., 2012; Pedrizzetti and Domenichini, 2005; Quarteroni et al., 2017; Seemann et al., 2019; Seo and Mittal, 2013). Later extending to artificial hearts as well as to other devices for physiologic support or for soft robotic devices (Cohrs et al., 2017; Kohll et al., 2019; Mao et al., 2020).

The cardiac ventricles reproduce the prototypes of a pumping system consisting of soft tissues. Their mechanical pumping function has always been described by the relationship between the pressure and the volume of the cardiac ventricles, where the infinitesimal mechanical work, dW, is given by the change of volume, dV, in the presence of pressure ($dW = pdV$). Such a classic approach leads to the definition of ventricular work as the pressure-volume (PV) loop area for the entire heartbeat (Berne and Levy, 1997).

The PV relationship represents the basic description of the mechanical function of a ventricle. It has the drawback of requiring invasive pressure measurement, which limited its extensive clinical application. Recently, simplifications of invasive procedures renewed the clinical interest in this PV analysis (Bastos et al., 2020); although it cannot be used in asymptomatic patients or massive screening protocols. For this reason, additional aspects of

* Corresponding author at: Department of Engineering and Architecture, University of Trieste, Italy.
E-mail address: giannip@dia.units.it (G. Pedrizzetti).

cardiac mechanics have been introduced in recent years to evaluate mechanical properties, such as the deformation pattern, in a non-invasive way by diagnostic imaging (Claus et al., 2015; Kaluzynski et al., 2001; Pedrizzetti et al., 2012).

The PV relationship takes into account the volume reduction/increase of the chamber at a given pressure. However, the volume is considered a single measure, and the approach does examine how the volumetric change is achieved. It is altogether evident that similar changes in volume values can be obtained through different phenomena depending on chamber's shape and its contraction/dilatation space-time pattern. Remarkably, the volumetric reduction corresponds to the development of blood flow, which can happen only in presence of a gradient of pressure between different regions of the chamber. The clinical relevance of blood flow patterns was witnessed in recent years using different imaging technologies (Kheradvar et al., 2019) and the significance of intraventricular pressure gradient demonstrated (Arvidsson et al., 2018; Eriksson et al., 2017; Lapinskas et al., 2019). This aspect is not included in the PV analysis.

This study aims to extend the description based on the PV relationship to include the role of the chamber's geometry, spatiotemporal deformation pattern and inlet/outlet flow. This information is achieved by extending the mathematical formulation of mechanical work to a second level of approximation, including the modulation of pressure gradients inside the chamber. This analysis initially sought to gain insights into the human heart's right ventricle function, which has a complex three-dimensional shape and is elusive to current visualization methods. Nevertheless, the approach has general validity and can be applied to different contexts. It is employed here to exemplary cases of normal and dysfunctional right ventricles.

2. Methods

2.1. Theory

In general, the rate of change of the mechanical work is the mechanical power, defined as the scalar product between force and velocity. In the case of a generic volume V of fluid with no volumetric forces, the only force is the pressure $p(t,\boldsymbol{x})$ (ignoring viscous stresses for the moment) that acts typically to its bounding surface S. The power, $\mathscr{P}(t)$, of this volume of fluid is

$$\mathscr{P}(t) = \int_S p\boldsymbol{n}\cdot\boldsymbol{v}dS = \int_V p\nabla\cdot\boldsymbol{v}dV + \int_V \nabla p\cdot\boldsymbol{v}dV. \tag{1}$$

where $\boldsymbol{v}(t,\boldsymbol{x})$ is the fluid velocity vector field, and $\boldsymbol{n}$ is the normal unit vector, directed outward. The second equality comes from the Gauss theorem, to underline the presence, in the definition (1), of a term (rightmost) that accounts for the power of the moving fluid.

At the basic level of approximation, when one assumes a constant pressure inside the ventricle $p(t,\boldsymbol{x}) \cong \bar{p}\,(t)$, Eq. (1) takes the simpler form

$$\mathscr{P}(t) \cong \bar{p}\int_S \boldsymbol{v}\cdot\boldsymbol{n}dS = \bar{p}\int_V \nabla\cdot\boldsymbol{v}dV = 0. \tag{2}$$

The expression (2) is globally zero for incompressibility in an isolated system where the power associated with the chamber's volumetric change is equivalent to that of the flow entering/exiting the chamber. This equivalence can be made explicit by expressing the absolute fluid velocity $\boldsymbol{v}$ as the sum of the geometric boundary's velocity plus the relative velocity of the fluid $\boldsymbol{v} = \boldsymbol{v}_b + \boldsymbol{v}_{fr}$, where the latter is nonzero only at the open valvular orifices. In this way, Eq. (2) can be expressed separating the two contributions

$$\mathscr{P}_0(t) = \bar{p}\int_S \boldsymbol{v}_b\cdot\boldsymbol{n}dS = -\bar{p}\int_S \boldsymbol{v}_{f_r}\cdot\boldsymbol{n}dS = \bar{p}\,\frac{dV}{dt}. \tag{3}$$

This formula is the well-known power (or volumetric power) required to achieve a volume reduction in the presence of a mean pressure $\bar{p}$, which, from mass conservation, is equivalent to the power required to eject flow against that pressure (and vice versa, during diastolic expansion and filling). The ventricle's associated mechanical work is the time integral of expression (3), which is the area of the PV loop when an entire heartbeat is considered.

The assumption of constant pressure inside the ventricle, leading to results (2) and (3), does not comply with the presence of a heterogeneous velocity patterns within the ventricle. The motion of blood can only be accounted by the presence of a pressure gradient, which means to consider the power associated to the blood flow inside the ventricular chamber, present in the last term of Eq. (1). Therefore, at an improved level of approximation, the pressure field at a generic point $\boldsymbol{x}$ is thus expressed by the average value, $\bar{p}\,(t)$ at the center, say $\boldsymbol{x} = 0$, plus the spatial modulation due to the average pressure gradient $\overline{\nabla p}$

$$p(t,\boldsymbol{x}) \cong \bar{p}\,(t) + \overline{\nabla p}(t)\cdot\boldsymbol{x}. \tag{4}$$

This approximation is increasingly valid until the chamber does not exhibit peculiar phenomena like narrow passages or protrusions having independent dynamics, and it is increasingly realistic in the flow dominated by unsteady phenomena. In these cases, the average pressure gradient is largely ascribed to global unsteadiness, which can be identified by low values of the Strouhal number, St. The flow in the heart chambers is characterized by $St\ 10^{-2}$, and assumption (4) was found to be realistic in several medical imaging recordings (Arvidsson et al., 2017; Cimino et al., 2012; Pedrizzetti et al., 2015; Töger et al., 2018). Substitution of (4) into (1) gives an additional term in the expression of mechanical power, which is related to the presence of a pressure gradient

$$\mathscr{P}_1(t) = \overline{\nabla p}\cdot\int_S \boldsymbol{x}(\boldsymbol{v}\cdot\boldsymbol{n})dS; \tag{5}$$

Expression (5) represents the mechanical power associated with flow motion driven by the pressure gradient, independently of the value of the average pressure $\bar{p}$. It includes the spatial distribution of the contraction patterns and -in global terms- it takes into account the role of fluid dynamics. This expression is thus associated with blood hemodynamics and we can be refer to it as the "hemodynamic power".

For the computation of $\mathscr{P}_1$ in formula (5), the average value of pressure gradient can be computed from the volume integral of fluid momentum inside the chamber (Domenichini and Pedrizzetti, 2016; Eriksson et al., 2016; Pedrizzetti et al., 2015; Töger et al., 2018)

$$\begin{aligned}\overline{\nabla p} &= \frac{\rho}{V}\int_V \left(\frac{\partial\boldsymbol{v}}{\partial t} + \boldsymbol{v}\cdot\nabla\boldsymbol{v}\right)dV \\ &= \frac{\rho}{V}\int_S \left[\boldsymbol{x}\left(\frac{\partial\boldsymbol{v}}{\partial t}\cdot\boldsymbol{n}\right) + \boldsymbol{v}(\boldsymbol{v}\cdot\boldsymbol{n})\right]dS;\end{aligned} \tag{6}$$

where ρ is the blood density and the second equality follows from the Gauss theorem (Pedrizzetti, 2019). In rigorous terms, expression (6) is an average force density, including the viscous stresses that, although commonly mostly negligible, are indirectly reintroduced at this stage. Expression (6) can be inserted into (5) to provide an explicit mean for computing the power associated with the intraventricular flow from the dynamic information of the bounding surface S.

2.2. Image acquisition and processing

The theoretical approach outlined above is evaluated in three cases of right ventricle (RV) acquired in adult subjects corresponding to a healthy volunteer and two patients with pressure and volumetric overload. Images are acquired by three-dimensional echocardiography performed with Vivid E95 (GE Healthcare, Horten, Norway). The study complies with the Declaration of Helsinki, and the Ethics Committee of the University of Trieste (protocol no. 0025052) approved it. Written informed consent of all registered volunteers was obtained.

Echocardiographic acquisitions were focused on the RV to achieve the maximum available frame rate, this ensured a number of volumes per heartbeat that ranges from 19 to 22. The collected images were then analyzed by 4D RV-Function 2.0 (TomTec Imaging Systems GmbH, Unterschleissheim, Germany) (Muraru et al., 2016). We carefully selected the tricuspid and pulmonary orifices as the inner edge of the respective annuli. The three-dimensional endocardial surface, which differentiates the tissue contour and the valvular boundary, was then exported as a triangulated mesh for further processing. The velocity of the geometric boundary, $\boldsymbol{v}_b$, was obtained by time differentiation of the boundary position. The fluid velocity at the tissue position and the closed orifices, coincided with the endocardial boundary velocity $\boldsymbol{v} = \boldsymbol{v}_b$. The additional relative fluid velocity at the open orifice (tricuspid at diastole, pulmonary at systole) was estimated by mass balance assuming a uniform distribution of the value perpendicular to the orifice boundary

$$\boldsymbol{v}_{f_r} \cong -\frac{\boldsymbol{n}}{S_{open}} \int_S \boldsymbol{v}_b \cdot \boldsymbol{n} dS; \tag{7}$$

where the fluid velocity is $\boldsymbol{v} = \boldsymbol{v}_b + \boldsymbol{v}_{f_r}$. Then the integrals in (5) and (6) are computed numerically by summing up each triangular element's contribution.

The power computed by (5) and (6) integrates the differential dynamics of the RV shape over the entire volumes. It, therefore, includes the effects of both the chamber size and its change in shape.

A first additional experiment was then performed to verify how the power was influenced by the effective value of the ventricular volumes. To this aim, the patients' RV geometry was artificially rescaled by a multiplicative factor to impose that both the end-systolic (ES) and the end-diastolic (ED) volumes coincided with those of the healthy subject. This result was achieved by rescaling the ES and ED patient's coordinates with a multiplicative factor given by the cubic root of the ratio between the healthy volumes and the corresponding patient's volumes. A linear relation between the ES and ED values extended the scaling factor to intermediate volume values to ensure continuity in time. The resulting patients' volume curves maintained the same time profile while they were scaled to match the normal ES and ED values, and the spatial contraction patter was not altered because the multiplicative factor was the same at all spatial positions.

A more extreme experiment was performed by transforming the patients' volume curve to have the entire time profiles identical to the healthy subject to verify how the global volumetric time variation influenced the computed power. This result was achieved starting from the previously scaled RV geometries and modulating the time during systolic contraction, and separately during diastolic expansion, to ensure the same time-varying profile. This drastic artificial change gave rise to three RVs with the same time profile of the volume curve and differed only in how the same volume variation was achieved through a different RV dynamic shape.

3. Results

The basic geometrical properties of the RV for the three subjects are reported in Table 1. The RV shape and the volume time profile are shown in Fig. 1. The volunteer (subject *a*) presented an overall healthy pattern with no clinical symptomatology despite a slight increase of atrial filling concerning early diastolic filling, which can be recognized by the slight sub-normal value of the vortex formation time (VFT) (Gharib et al., 2006). Both patients presented a volumetric increase, reduction of ejection fraction compensated by an increase of the stroke volume. One of them (subject *b*) had a moderated RV dilatation and light clinical dysfunction following a volume overload due to severe pulmonary valve regurgitation. This patient showed a diastolic dysfunction with intense early filling and almost absent atrial filling leading an apparently normal value of VFT. The other patient (subject *c*) presented a severe dilatation and moderate RV dysfunction, pulmonary embolism and pressure overload. The diastolic function presents a drastic reduction of VFT despite a normalized time profile of RV filling.

The time profile of the power associated with flow development, normalized with the volume, $\mathscr{P}_1(t)/V(t)$, is reported in Fig. 2 for the three subjects. The healthy subject presented the development of power wave during the early phase of the systolic ejection, indicating that the pressure gradient was directed toward the outflow tract, aligned with the direction of velocity and effective at creating the outflow. Diastole displayed a balance between the power of the incoming flow and the receiving compliance by the tissue; a slight excess of the incoming of power was noticed during atrial filling. The first patient featured an irregular growth of the ejective power due to the asynchronous development of pressure gradients associated with altering the spatial contraction pattern of the RV walls. The sharp spike in diastolic flow indicated the imbalance between the power of inflow and wall compliance. The second patient presented a weak systolic power limited to the very early phase of the ejection and biphasic waves during diastole, suggesting that (positive) tissue relaxation anticipates the incoming flow power and the (negative) power of inflow faces a non-compliant (previously expanded) chamber.

The supplemental videos 1 to 3 show the beating RV shape with an indication of the instantaneous position on the time profiles of the volume and of the power associated with the spatial distribution of pressure gradient.

The results from the first experiment, where the patients' chamber was rescaled to have the same ES and ED volumes of the normal subject, are shown in Fig. 3. The comparison with the previous Fig. 2 shows that the normalized power curves are almost identical, with minimal differences due to the stroke volume change. These outcomes demonstrated that the absolute volume values had small influence on the power distribution once it was normalized with the volume; although the normalization did not compensate entirely for volumes, as the stroke value also had an influence.

The results from the second more drastic experiment, where all subjects were brought to have identical volume curves, are shown in Fig. 4. As could be expected, the power curves presented more similar behavior, with one systolic and two diastolic waves. Nevertheless, significant differences remained. The two patients' curves presented a significantly lower systolic ejection power than the healthy subjects, and the biphasic diastolic waves remained well noticeable in the second patient. It should be remarked that all indicators based on volumetric properties were identical, and the remaining differences were only imputable to the differential shape dynamics in the RV chamber.

Table 1
Volumetric characteristics of right ventricle in the analyzed subjects. Legend: EDV = end-diastolic volume; ESV = end-systolic volume; SV = stroke volume; EF = ejection fraction; VFT = vortex formation time.

		EDV [cm^3]	ESV [cm^3]	SV [cm^3]	EF [%]	VFT [–]
(*a*)	Normal	78.8	33.3	45.5	58	3.4
(*b*)	Dilated Chamber Volume Overload	153.5	84.6	68.9	45	4.0
(*c*)	Dilated Chamber Pressure Overload	195.0	124.1	70.9	36	0.8

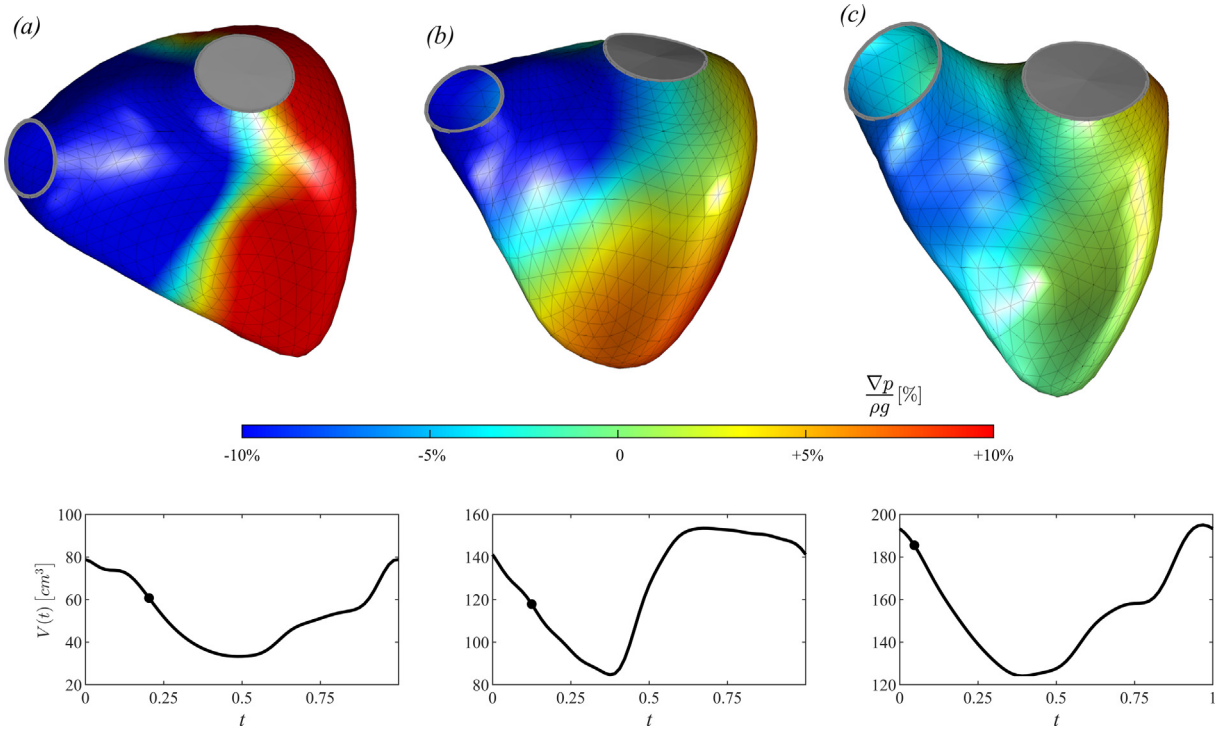

Fig. 1. For each of the three subjects analyzed: (*a*) normal subject, (*b*) patient with volume overload, (*c*) patient with pressure overload. The upper row shows the three-dimensional shape of the right ventricles, the lower row draws, and the time course of the corresponding ventricular volume, time zero is set at end-diastole (assumed as the instant when volume is maximum). The selected instant of ventricular shape corresponds to the peak systolic power as indicated with dot in the volume curve. The ventricle is colored by the pressure gradient vector, normalized with density, and expressed as a percentage of gravity acceleration, $\overline{\nabla p}/\rho g$, as indicated by the colormap.

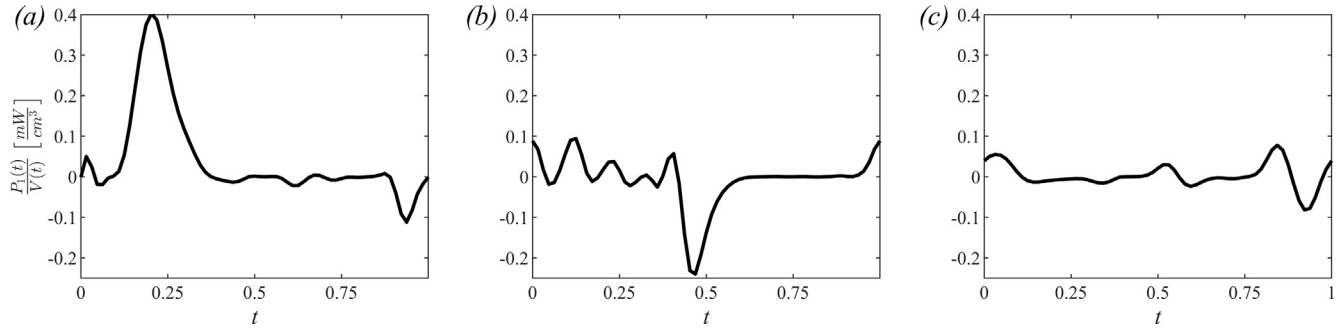

Fig. 2. For each of the three subjects analyzed (*a,b,c*), the curves draw the power's time course, normalized with volume, associated with flow and pressure gradient.

4. Discussion

A significant challenge in cardiology nowadays is improving the ability to reveal early subclinical changes in cardiac function well before the cardiac tissues have undergone irreversible modification, similarly, revealing subclinical improvements that can anticipate a therapy's effectiveness. Here a duty of engineering and physics scientists is about defining physics-based properties capable of characterizing the cardiac pump's function in depth. Along this line, this study introduces the concept of mechanical power that provides a measure of ventricular function based on first physical principles.

During the last decade, a significant amount of clinical work focused on evaluating myocardial deformation, which eventually allowed recognizing that a reduction of longitudinal deformation (strain) in the left ventricle (LV) was often associated to early

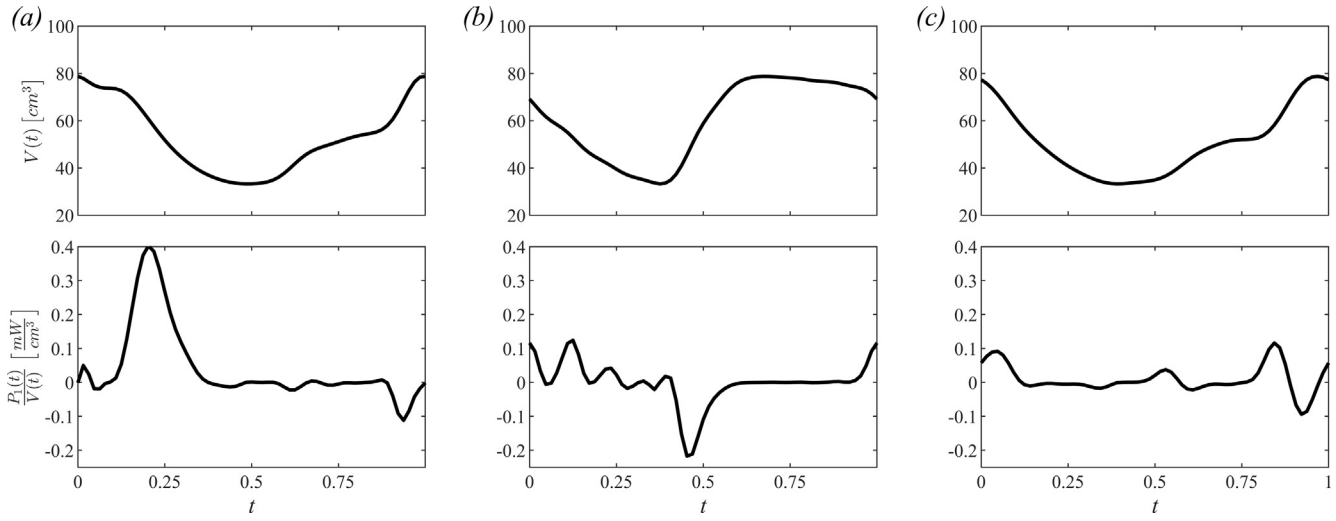

Fig. 3. Same as Fig. 2, where the ventricular geometry of the two patients (*b*) and (*c*) has been artificially altered to ensure the same end-systole and end-diastolic volumes as for the healthy subjects (*a*).

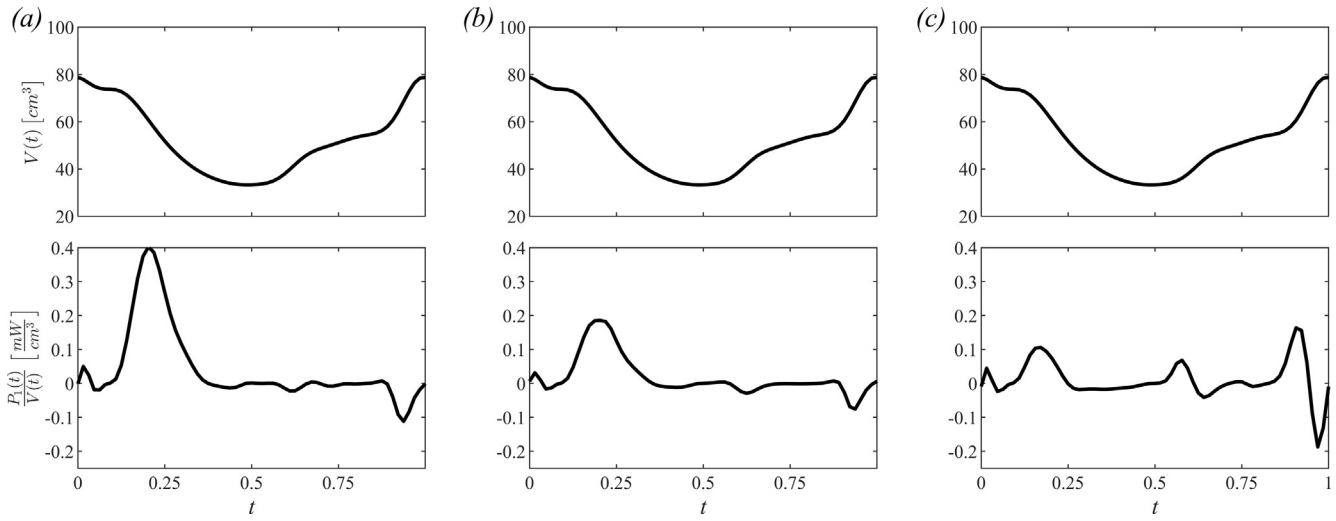

Fig. 4. Same as Fig. 2, where the ventricular geometry of the two patients (*b*) and (*c*) has been artificially altered to ensure the same time course of the volume time curve, which is identical to the one of healthy subjects (*a*).

stages hypertrophic remodeling (Claus et al., 2015; Schuster et al., 2016). At the same time, numerous studies based on numerical simulation, conceptual models, or biophysical analysis, suggested that an alteration of LV fluid dynamics could be associate with early changes in cardiac function (Abe et al., 2013; Eriksson et al., 2013; Gharib et al., 2006; Harfi et al., 2017; Pasipoularides, 2015a, 2015b; Pedrizzetti et al., 2014; Pedrizzetti and Domenichini, 2015). In particular, the intra-ventricular pressure gradient or the hemodynamic force vector (which is the integral of pressure gradient over the ventricular chamber) was recognized as a clinical biomarker of LV function and even anticipated the development of ventricular remodeling (Arvidsson et al., 2018; Eriksson et al., 2017; Guerra et al., 2013; Pedrizzetti et al., 2015). The application of these flow-based concepts to the LV made advantage of the base-apex direction as a geometrical reference, whereas application to chambers with complex geometry, such as the RV, is difficult for the absence of a dominant direction.

This study introduced an original physics-based synthesis where the intraventricular pressure gradient development is weighted with its ability to increase blood flow. The hemodynamic power, given by expressions (5) and (6), considers the spatial contraction pattern and how it matches with flow forces, thus providing a parameter that is incremental to volumetric measurements. Hemodynamic power is a scalar property that can be evaluated non-invasively from image processing capable of segmenting the chamber boundary. Moreover, being a scalar property, it is independent of the shape of the cardiac chamber and the relative orientation of the inflow and outflow tracks.

The complex RV contraction pattern results from different components summarized as longitudinal shortening, the differential radial motion of either free wall and septum, anteroposterior stretching, and the free wall over the septum whose alterations are difficult to detect (Kovács et al., 2019). These preliminary results demonstrated a reduction of the ejection power in both patients with volumetric dilatation; this phenomenon may be partially imputable to the loss of the peristaltic-like contribution to contraction associated with the changes in RV myocardial architecture due to dilatation (Buckberg and Hoffman, 2014). The patient

with pressure overload reveals an abnormal filling pattern that may be imputable to the wall rigidity increase. The additional experiments provided preliminary support that the hemodynamic power can show minor alterations in the chamber's dynamic shape regardless of its volume.

In summary, amplitude and time course of hemodynamic power (HDP) provide information on the efficient coupling between tissue contraction pattern, development of pressure gradient and generation of blood flow, which is turn influences active and passive wall stresses. So, HDP may be an early indicator of subclinical chamber dysfunction, before changes in volumetric measures have occurred. Clinically, HPD curve can be assessed by 3D endocardial surfaces obtained by common image analysis in both cardiac magnetic resonance and echocardiography.

The approach proposed here has general validity and can be extended to general pumping devices made of soft material. It can be applied to evaluate chambers' performance in artificial hearts and other devices for physiologic support or soft robotic devices (Cohrs et al., 2017; Kohll et al., 2019; Mao et al., 2020).

5. Conclusion

The hemodynamic power introduced in this study represents a physics-based measure accounting for the space-time dynamical motion pattern of soft-tissue pumping chambers. Preliminary results demonstrated its significant alteration in dysfunctional right ventricles independently of volumetric measures, thus suggesting a role for detecting dysfunctions at a subclinical, early stage. Systematic evaluations are required to verify its validity in the clinical context. The present work provides the engineering background for future clinical studies.

Declaration of Competing Interest

The authors declare that they have no known competing financial interests or personal relationships that could have appeared to influence the work reported in this paper.

Acknowledgments

Author GP acknowledges partial support for this study by the Italian Ministry of Education and Research under project PRIN 2017 A889FP.

References

Abe, H., Caracciolo, G., Kheradvar, A., Pedrizzetti, G., Khandheria, B.K., Narula, J., Sengupta, P.P., 2013. Contrast echocardiography for assessing left ventricular vortex strength in heart failure: A prospective cohort study. Eur. Heart J. Cardiovasc. Imaging 14, 1049–1060. https://doi.org/10.1093/ehjci/jet049.

Arvidsson, P.M., Töger, J., Carlsson, M., Steding-Ehrenborg, K., Pedrizzetti, G., Heiberg, E., Arheden, H., 2017. Left and right ventricular hemodynamic forces in healthy volunteers and elite athletes assessed with 4D flow magnetic resonance imaging. Am. J. Physiol. - Hear. Circ. Physiol. 312 (2), H314–H328. https://doi.org/10.1152/ajpheart.00583.2016.

Arvidsson, P.M., Töger, J., Pedrizzetti, G., Heiberg, E., Borgquist, R., Carlsson, M., Arheden, H., 2018. Hemodynamic forces using 4D flow MRI: an independent biomarker of cardiac function in heart failure with left ventricular dyssynchrony? Am. J. Physiol. Circ. Physiol. ajpheart.00112.2018. Doi: 10.1152/ajpheart.00112.2018

Baillargeon, B., Rebelo, N., Fox, D.D., Taylor, R.L., Kuhl, E., 2014. The living heart project: A robust and integrative simulator for human heart function. Eur. J. Mech. A/Solids 48, 38–47. https://doi.org/10.1016/j.euromechsol.2014.04.001.

Bastos, M.B., Burkhoff, D., Maly, J., Daemen, J., Den Uil, C.A., Ameloot, K., Lenzen, M., Mahfoud, F., Zijlstra, F., Schreuder, J.J., Van Mieghem, N.M., 2020. Invasive left ventricle pressure-volume analysis: Overview and practical clinical implications. Eur. Heart J. 41, 1286–1297. https://doi.org/10.1093/eurheartj/ehz552.

Berne, R.M., Levy, M.N., 1997. Cardiovascular Physiology. Mosby-Year Book Inc, St. Louis.

Buckberg, G., Hoffman, J.I.E., 2014. Right ventricular architecture responsible for mechanical performance: Unifying role of ventricular septum. J. Thorac. Cardiovasc. Surg. 148 (6), 3166–3171.e4. https://doi.org/10.1016/j.jtcvs.2014.05.044.

Cimino, S., Pedrizzetti, G., Tonti, G., Canali, E., Petronilli, V., De Luca, L., Iacoboni, C., Agati, L., 2012. In vivo analysis of intraventricular fluid dynamics in healthy hearts. Eur. J. Mech. B/Fluids 35, 40–46. https://doi.org/10.1016/j.euromechflu.2012.03.014.

Claus, P., Omar, A.M.S., Pedrizzetti, G., Sengupta, P.P., Nagel, E., 2015. Tissue tracking technology for assessing cardiac mechanics: principles, normal values, and clinical applications. JACC Cardiovasc. Imaging 8 (12), 1444–1460. https://doi.org/10.1016/j.jcmg.2015.11.001.

Cohrs, N.H., Petrou, A., Loepfe, M., Yliruka, M., Schumacher, C.M., Kohll, A.X., Starck, C.T., Schmid Daners, M., Meboldt, M., Falk, V., Stark, W.J., 2017. A soft total artificial heart—first concept evaluation on a hybrid mock circulation. Artif. Organs 41 (10), 948–958. https://doi.org/10.1111/aor.12956.

Domenichini, F., Pedrizzetti, G., 2016. Hemodynamic forces in a model left ventricle. Phys. Rev. Fluids 1,. https://doi.org/10.1103/PhysRevFluids.00.003200 083201.

Eriksson, J., Bolger, A.F., Ebbers, T., Carlhäll, C.-J., 2016. Assessment of left ventricular hemodynamic forces in healthy subjects and patients with dilated cardiomyopathy using 4D flow MRI. Physiol. Rep. 4, 741–747. https://doi.org/10.14814/phy2.12685.

Eriksson, J., Bolger, A.F., Ebbers, T., Carlhäll, C.J., 2013. Four-dimensional blood flow-specific markers of LV dysfunction in dilated cardiomyopathy. Eur. Heart J. Cardiovasc. Imaging. Doi: 10.1093/ehjci/jes159

Eriksson, J., Zajac, J., Alehagen, U., Bolger, A.F., Ebbers, T., Carlhäll, C.-J., 2017. Left ventricular hemodynamic forces as a marker of mechanical dyssynchrony in heart failure patients with left bundle branch block. Sci. Rep. 7, 2971. https://doi.org/10.1038/s41598-017-03089-x.

Gharib, M., Rambod, E., Kheradvar, A., Sahn, D.J., Dabiri, J.O., 2006. Optimal vortex formation as an index of cardiac health. Proc. Natl. Acad. Sci. 103, 6305–6308. Doi: 10.1073/pnas.0600520103

Guerra, M., Brás-Silva, C., Amorim, M.J., Moura, C., Bastos, P., Leite-Moreira, A.F., 2013. Intraventricular pressure gradients in heart failure. Physiol. Res. 62, 479–487.

Harfi, T.T., Seo, J. hee, Yasir, H.S., Welsh, N., Mayer, S.A., Abraham, T.P., George, R.T., Mittal, R., 2017. The E-wave propagation index (EPI): A novel echocardiographic parameter for prediction of left ventricular thrombus. Derivation from computational fluid dynamic modeling and validation on human subjects. Int. J. Cardiol. Doi: 10.1016/j.ijcard.2016.10.079

Kaluzynski, K., Chen, X., Emelianov, S.Y., Skovoroda, A.R., O'Donnell, M., 2001. Strain rate imaging using two-dimensional speckle tracking. IEEE Trans. Ultrason. Ferroelectr. Freq. Control 48, 1111–1123. https://doi.org/10.1109/58.935730.

Kheradvar, A., Rickers, C., Morisawa, D., Kim, M., Hong, G.-R., Pedrizzetti, G., 2019. Diagnostic and prognostic significance of cardiovascular vortex formation. J. Cardiol. 74 (5), 403–411. https://doi.org/10.1016/j.jjcc.2019.05.005.

Kohll, A.X., Cohrs, N.H., Walker, R., Petrou, A., Loepfe, M., Schmid Daners, M., Falk, V., Meboldt, M., Stark, W.J., 2019. Long-term performance of a pneumatically actuated soft pump manufactured by rubber compression molding. Soft Robot. 6 (2), 206–213. https://doi.org/10.1089/soro.2018.0057.

Kovács, A., Lakatos, B., Tokodi, M., Merkely, B., 2019. Right ventricular mechanical pattern in health and disease: beyond longitudinal shortening. Heart Fail. Rev. 24, 511–520. Doi: 10.1007/s10741-019-09778-1

Lapinskas, T., Pedrizzetti, G., Stoiber, L., Düngen, H.D., Edelmann, F., Pieske, B., Kelle, S., 2019. The Intraventricular Hemodynamic Forces Estimated Using Routine CMR Cine Images: A New Marker of the Failing Heart. JACC Cardiovasc. Imaging. Doi: 10.1016/j.jcmg.2018.08.012

Mao, Z., Nagaoka, T., Yokota, S., Kim, J.wan., 2020. Soft fiber-reinforced bending finger with three chambers actuated by ECF (electro-conjugate fluid) pumps. Sens. Actuators, A Phys. 310,. https://doi.org/10.1016/j.sna.2020.112034 112034.

Muraru, D., Spadotto, V., Cecchetto, A., Romeo, G., Aruta, P., Ermacora, D., Jenei, C., Cucchini, U., Iliceto, S., Badano, L.P., 2016. New speckle-tracking algorithm for right ventricular volume analysis from three-dimensional echocardiographic data sets: validation with cardiac magnetic resonance and comparison with the previous analysis tool. Eur. Hear. J. – Cardiovasc. Imaging 17, 1279–1289. Doi: 10.1093/ehjci/jev309

Pasipoularides, A., 2015a. Mechanotransduction mechanisms for intraventricular diastolic vortex forces and myocardial deformations: Part 2. J. Cardiovasc. Transl. Res. 8, 293–318. Doi: 10.1007/s12265-015-9630-8.

Pasipoularides, A., 2015b. Mechanotransduction mechanisms for intraventricular diastolic vortex forces and myocardial deformations: part 1. J. Cardiovasc. Transl. Res. 8, 76–87. Doi: 10.1007/s12265-015-9611-y

Pedrizzetti, G., 2019. On the computation of hemodynamic forces in the heart chambers. J. Biomech. Doi: 10.1016/j.jbiomech.2019.109323

Pedrizzetti, G., Domenichini, F., 2015. Left ventricular fluid mechanics: the long way from theoretical models to clinical applications. Ann. Biomed. Eng. 43, 26–40. Doi: 10.1007/s10439-014-1101-x

Pedrizzetti, G., Domenichini, F., 2005. Nature optimizes the swirling flow in the human left ventricle. Phys. Rev. Lett. 95, 1–4. https://doi.org/10.1103/PhysRevLett.95.108101.

Pedrizzetti, G., Kraigher-Krainer, E., De Luca, A., Caracciolo, G., Mangual, J.O.J.O., Shah, A., Toncelli, L., Domenichini, F., Tonti, G., Galanti, G., Sengupta, P.P.P., Narula, J., Solomon, S., 2012. Functional strain-line pattern in the human left ventricle. Phys. Rev. Lett. 109,. https://doi.org/10.1103/PhysRevLett.109.048103 048103.

Pedrizzetti, G., La Canna, G., Alfieri, O., Tonti, G., 2014. The vortex - An early predictor of cardiovascular outcome? Nat. Rev. Cardiol. 11. Doi: 10.1038/nrcardio.2014.75

Pedrizzetti, G., Martiniello, A.R., Bianchi, V., D'Onofrio, A., Caso, P., Tonti, G., D'Onofrio, A., Caso, P., Tonti, G., 2015. Cardiac fluid dynamics anticipates heart adaptation. J. Biomech. 48, 388–391. https://doi.org/10.1016/j.jbiomech.2014.11.049.

Quarteroni, A., Lassila, T., Rossi, S., Ruiz-Baier, R., 2017. Integrated heart—coupling multiscale and multiphysics models for the simulation of the cardiac function. Comput. Methods Appl. Mech. Eng. 314, 345–407. https://doi.org/10.1016/j.cma.2016.05.031.

Schuster, A., Hor, K.N., Kowallick, J.T., Beerbaum, P., Kutty, S., 2016. Cardiovascular magnetic resonance myocardial feature tracking: concepts and clinical applications. Circ. Cardiovasc. Imaging 9,. https://doi.org/10.1161/CIRCIMAGING.115.004077 e004077.

Seemann, F., Arvidsson, P., Nordlund, D., Kopic, S., Carlsson, M., Arheden, H., Heiberg, E., 2019. Noninvasive quantification of pressure-volume loops from brachial pressure and cardiovascular magnetic resonance. Circ. Cardiovasc. Imaging 12,. https://doi.org/10.1161/CIRCIMAGING.118.008493 e008493.

Seo, J.H., Mittal, R., 2013. Effect of diastolic flow patterns on the function of the left ventricle. Phys. Fluids. Doi: 10.1063/1.4819067.

Töger, J., Arvidsson, P.M., Bock, J., Kanski, M., Pedrizzetti, G., Carlsson, M., Arheden, H., Heiberg, E., 2018. Hemodynamic forces in the left and right ventricles of the human heart using 4D flow magnetic resonance imaging: Phantom validation, reproducibility, sensitivity to respiratory gating and free analysis software. PLoS One 13. Doi: 10.1371/journal.pone.0195597.